THE ASTROPHYSICAL JOURNAL, 526:27–39, 1999 November 20

OPTICAL-RADIO ALIGNMENT IN COMPACT STEEP-SPECTRUM RADIO SOURCES

W. H. DE VRIES,[1] C. P. O'DEA, AND S. A. BAUM
Space Telescope Science Institute, 3700 San Martin Drive, Baltimore, MD 21218

AND

P. D. BARTHEL
Kapteyn Astronomical Institute, P.O. Box 800, NL-9700 AV, Groningen, The Netherlands
Received 1998 December 2; accepted 1999 July 9

ABSTRACT

We discuss *Hubble Space Telescope* (*HST*) WFPC2 observations through the broad red filter F702W of 30 3CR sources from the Compact Steep Spectrum (CSS) radio source sample, and present 11 new *HST*/WFPC2 images through linear ramp filters (LRF), isolating either rest-frame [O II] 3727 Å or [O III] 5007 Å radiation. In nearly all the CSS galaxies, we find high surface brightness emission that is aligned with the radio axis. The strong nuclear PSF prevents us from detecting such aligned light at similar levels in most of the CSS quasars. However, a comparison between CSS galaxies and quasars with PSF signatures removed reveals no inconsistency with the viewing angle unification scheme. The alignment effect in CSS sources is not a strong function of redshift, and is seen over the entire redshift range of the sample ($0.2 \lesssim z \lesssim 1.5$). Our analysis of the LRF images and complementary KPNO spectroscopy reveals that the aligned light is predominantly emission-line gas. These observations demonstrate the existence of dense gas in the host galaxies of CSS sources, strongly interacting with the expanding radio sources. Assuming such a shock interaction, cooling-time arguments suggest that lobe expansion speeds of $\gtrsim 1000$ km s^{-1} and ambient densities of ~ 1 cm^{-3} are consistent with the observed offset between the leading edge of the radio lobe and the optical line emission.

Subject headings: galaxies: active — galaxies: structure — quasars: emission lines — radio continuum: galaxies

1. INTRODUCTION

Compact steep-spectrum (CSS) sources form an interesting class of powerful radio sources. These sources, which are defined to have a maximum projected size[2] of subgalactic dimension (20 kpc; Fanti et al. 1990), are believed to form the intermediate stage in radio source evolution. In this scenario, powerful radio sources are "born" as GHz peaked-spectrum radio sources (GPS; O'Dea, Baum, & Stanghellini 1991; O'Dea 1998), with a typical radio source size $\lesssim 1$ kpc; they subsequently expand into galactic-size structures (the CSS phase), and finally into the large-scale Fanaroff-Riley class I and II radio sources. Models for this evolutionary scenario have been put forward by several authors over the years, e.g., Carvalho (1985), Mutel, Su, & Song (1990), De Young (1993, 1997), Fanti et al. (1995), Readhead et al. (1996a, 1996b), Begelman (1996), and Bicknell, Dopita, & O'Dea (1997, hereafter BDO97). Constraints from relative numbers of large and small sources rule out evolution with both a constant expansion velocity and constant radio luminosity. Instead, the data are consistent with a scenario in which the sources decrease in radio luminosity as they expand from GPS to large-scale radio sources (e.g., O'Dea & Baum 1997).

In addition to unifying the radio properties, the evolutionary sequence has implications for the underlying host galaxy. The very different evolutionary timescales for galaxy populations and radio sources (Gyr versus Myr) imply that the host galaxy properties should be independent of radio source size or, equivalently, age. Indeed, host galaxy absolute magnitudes and colors have been found to be similar in the near infrared (de Vries et al. 1998a, 1998b). Another consequence of the evolutionary scheme is that effects linked to the radio source expanding in the host ISM should be present at all stages, albeit perhaps at different levels. For instance, some large-scale sources are found to exhibit the alignment effect (optical and radio symmetry axes have the same position angle), e.g., Chambers, Miley, & van Breugel (1987) and McCarthy et al. (1987). Therefore the more compact sources, where the level of interaction between the radio plasma and the ambient medium is expected to be higher, should show the alignment effect as well. BDO97 present a model that attempts to unify the optical and radio properties of compact radio sources (see also Begelman 1998 for a similar model).

The BDO97 model makes at least one testable prediction. The expanding radio source should shock-ionize the ambient medium, producing copious amounts of line emission, which is aligned by its very nature. The source class most suited for testing this prediction is the CSS class. The GPS radio sources are too small ($\lesssim 0\farcs1$) to be successfully resolved in the optical even by *Hubble Space Telescope* (*HST*). In addition, since the radio is still subkiloparsec in size, any associated emission lines will be subject to obscuration from dust and gas in the circumnuclear region. On the other hand, in the FR II sources the radio structure has expanded beyond the host galaxy; therefore, any observable interaction by the radio plasma will be with matter outside the host galaxy (e.g., with satellite galaxies or cluster gas), something not accounted for in the model.

In a previous paper (de Vries et al. 1997, hereafter Paper I), we presented *HST* Planetary Camera 2 (WFPC2) images of 30 CSS sources, taken in the F702W filter (a broad *R* band). Radio structures from the literature were overlaid to permit radio-optical structural comparisons. In this paper

[1] Also at Kapteyn Astronomical Institute.
[2] We use $H_0 = 75$ km s^{-1} Mpc^{-1} and $q_0 = 0.5$ throughout this paper.

we will discuss these results. Furthermore, we present rest-frame [O III] 5007 Å (and in some cases [O II] 3727 Å) emission-line images of some of the sources in order to investigate the nature of the aligned component.

2. THE F702W *HST* DATA

An account of the reduction of the data and a discussion of individual sources can be found in Paper I. Here we summarize the selection criteria of the sample of highly luminous CSS sources. Our sample is drawn from the Fanti et al. (1990) compilation, defined as having a projected largest linear size $\lesssim 20$ kpc, a flux density at 178 MHz > 10 Jy, a Galactic latitude $|b| > 10°$, a declination $\delta > +10$, and a monochromatic radio power $\log (P_{178}) > 26.5$ W Hz^{-1} (this effectively excludes FR I type radio sources). Our sample consists of the 3CR sources in the Fanti et al. list that were observed by the WFPC2 snapshot survey (de Koff et al. 1996; McCarthy et al. 1997), and consists of 14 galaxies ($0.16 \lesssim z \lesssim 1.28$) and 16 quasars ($0.32 \lesssim z \lesssim 1.96$). A histogram of the redshift distribution can be found in Paper I (Fig. 1), while a complete list of the sample sources and the results from the F702W photometry is given in Table 1.

Since the compilation of the initial CSS list by Fanti et al. (1990), evidence belying their CSS nature has been found for some sources. A few sources have diffuse radio halos that are larger than the 20 kpc cutoff, e.g., 3C 216 (e.g., Barthel, Pearson, & Readhead 1988; Taylor, Ge, & O'Dea 1995) and 3C 380 (e.g., Wilkinson 1990; van Breugel et al. 1992). Other sources may appear small because of an orientation close to perpendicular to the plane of the sky, e.g., possibly 3C 147 and 3C 346 (Dey & Van Breugel 1994; Cotton et al. 1995). The source 3C 213.1 has a lobe separation of 26 kpc, and should be categorized as a small FR II. Finally, the source 3C 299 is found to be part of a large, very asymmetric radio source, the CSS component being the northeastern lobe (see Liu & Pooley 1991; van Breugel et al. 1992). In the CSS source statistics, these sources are treated separately.

3. INTERPRETATION OF THE BROADBAND F702W DATA

3.1. *Alignment Classification*

Based on the overlay between the *HST* optical images and the radio structures (Paper I), we classify the optical-radio alignment in three ways: (1) detailed correspondence, (2) global correspondence, and (3) undefined. The first class

TABLE 1

F702W OBSERVATIONAL RESULTS

3CR Designation	Type[a]	z	m_{tot}[b]	m_{core}[c]	F_{core}/F_{total}[d]	m_{ext}[e]	Δ[f] (deg)
3C 43	Q	1.459	20.59 ± 0.01	20.88	0.77 ± 0.05	23.39	
3C 49	G	0.621	20.70 ± 0.03	22.60	0.17 ± 0.01	20.91	−10
3C 67	G	0.310	18.77 ± 0.01	19.35	0.59 ± 0.04	19.73	−5
3C 93.1	G	0.243	19.11 ± 0.01	20.17	0.38 ± 0.02	19.62	
3C 119	G	1.023	20.20 ± 0.01	20.43	0.81 ± 0.05	22.00	
3C 138	Q	0.759	18.48 ± 0.01	18.70	0.82 ± 0.05	22.26	−23
3C 147[g]	Q	0.545	17.21 ± 0.01	17.45	0.80 ± 0.05	20.24	
3C 186	Q	1.063	17.49 ± 0.01	17.69	0.83 ± 0.05	23.54	
3C 190	Q	1.195	18.92 ± 0.01	19.13	0.82 ± 0.05	23.78	
3C 191	Q	1.956	17.80 ± 0.01	18.00	0.83 ± 0.05	22.73	
3C 213.1	G	0.194	17.75 ± 0.01	19.15	0.28 ± 0.02	18.10	33
3C 216[g]	Q	0.670	18.80 ± 0.01	19.14	0.73 ± 0.05	20.23	−4
3C 237	G	0.877	21.08 ± 0.03	22.12	0.45 ± 0.03	21.73	0
3C 258	G	0.165	19.61 ± 0.02	20.89	0.31 ± 0.02	20.01	
3C 266	G	1.275	21.25 ± 0.1	23.76	0.10 ± 0.01	21.36	−13
3C 268.3	G	0.371	20.19 ± 0.02	21.55	0.29 ± 0.02	20.56	8
3C 277.1	Q	0.321	17.66 ± 0.01	18.02	0.72 ± 0.05	19.03	0
3C 286	Q	0.849	17.45 ± 0.01	17.80	0.72 ± 0.05	18.85	
3C 287	Q	1.055	17.47 ± 0.01	17.69	0.82 ± 0.05	21.61	
3C 298	Q	1.436	16.45 ± 0.01	16.70	0.79 ± 0.05	19.74	
3C 299[g]	G	0.367	19.64 ± 0.1	21.80	0.14 ± 0.02	19.80	8
3C 303.1	G	0.267	18.73 ± 0.01	20.20	0.26 ± 0.02	19.05	−10
3C 305.1	G	1.132	21.18 ± 0.05	23.56	0.12 ± 0.01	21.31	−12
3C 309.1	Q	0.905	17.06 ± 0.01	17.30	0.80 ± 0.05	20.48	
3C 343	Q	0.988	20.04 ± 0.02	21.62	0.23 ± 0.02	20.33	
3C 343.1	G	0.750	20.93 ± 0.03	22.67	0.20 ± 0.01	21.17	9
3C 346[g]	G	0.161	18.37 ± 0.03	18.78	0.69 ± 0.04	19.63	0
3C 380[g]	Q	0.692	16.86 ± 0.01	17.10	0.80 ± 0.05	20.07	0
3C 454	Q	1.757	18.42 ± 0.01	18.71	0.77 ± 0.05	21.08	
3C 455	Q?	0.543	19.91 ± 0.02	20.83	0.43 ± 0.03	20.52	11

NOTE.—The quasar 3C 455 should possibly be reclassified as a galaxy because of its narrow permitted lines (GW94) and the very weak radio core (Bogers et al. 1994).

[a] Q: quasar; G: galaxy.

[b] *HST* F702W magnitude, with formal fitting error.

[c] Magnitude inside a 1 kpc radius ($H_0 = 75$ km s^{-1} Mpc^{-1}, $q_0 = 0.5$).

[d] Fraction of total flux inside a 1 kpc radius.

[e] Calculated magnitude outside the 1 kpc radius.

[f] Alignment angle, with a typical uncertainty of 5°.

[g] Source is larger than the 20 kpc cutoff for CSS sources.

contains sources with a one-to-one relation between their optical and radio structures, possibly due to optical synchrotron emission from radio hot spots and jets. This is found in the sources 3C 213.1, 3C 346, and 3C 380. Detailed correspondence does not imply, however, that globally the angle between radio and optical emission is small (see 3C 213.1). Therefore, without the detection of optical hot spot emission, these sources would be characterized as rather poorly aligned or even misaligned. In addition, it should be noted that all sources in this class are probably not true CSS sources, each one of them being larger than the 20 kpc cutoff size. The present shallow observations do not permit us to determine whether optical synchrotron emission is present in true CSS sources.

We find a group of sources displaying global alignment, in which the optical and radio symmetry axes are aligned within $\sim 15°$. No detailed correspondence between radio and optical emission structures is present. In most of our images, the aligned light lies within the radio source extent. However, we find two sources, 3C 343.1 and possibly 3C 237, in which the aligned light extends beyond the radio source (Axon et al. 1999 find four more). For sources in the "undefined" category, no alignment angle measurement is possible. This is the case for the heavily PSF-dominated sources (almost all quasars, and 3C 119, reclassified as a galaxy by Eracleous & Halpern 1994). Subtraction of model PSFs yielded little or no extended emission, so we were unable to measure an alignment angle in these cases.

The results of this classification are listed in Table 2, while the alignment angles are given in Table 1. The distinction between the galaxies, which are on average (globally) aligned, and the quasars, for which alignment cannot be measured, is readily apparent.

We see no significant variation in alignment angle with redshift in the CSS sources (Fig. 1 and Table 1). Ignoring the detailed correspondence sources (the triangles in the plot), which are too large to be true CSS sources, the alignment is within 20° at all redshifts. This is comparable to the alignment of large-scale FR II sources, provided that the alignment is detected using narrowband filters centered on rest-frame emission lines (McCarthy & van Breugel 1989; McCarthy, Spinrad, & van Breugel 1995). Continuum radiation alignment is rarely seen at redshifts below ~ 0.6, as is clearly demonstrated in Figure 2 (*middle histogram*). This is a first indication that the alignment in CSS sources is mainly due to line-emitting gas (cf. § 6). In contrast to the [O II] emission-line data (Fig. 2, *top histogram*), which are

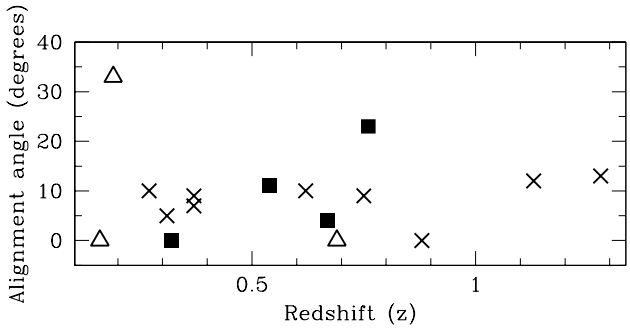

FIG. 1.—Radio-optical alignment angle vs. redshift. The filled squares represent the quasars and the crosses the galaxies. The detailed correspondence sources (3C 346, 3C 213.1, and 3C 380, *left to right*) are indicated by the open triangles, since their radio sizes exceed the CSS limit.

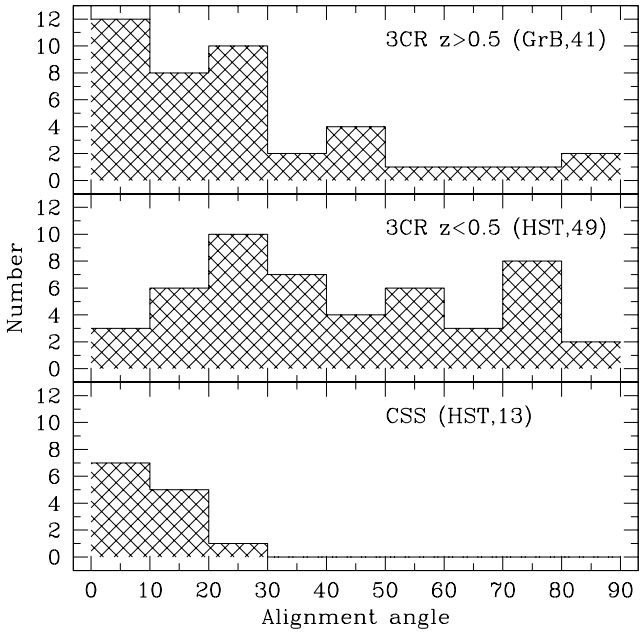

FIG. 2.—Histogram of the alignment angle distribution for 3CR sources at redshifts larger than 0.5 (*top*), 3CR sources at redshifts lower than 0.5 (*middle*), and the CSS sources in our sample (*bottom*). The high-redshift 3CR data are based on ground-based [O II] imaging (McCarthy et al. 1995), whereas both the low-z 3CR and the CSS histograms are based on *HST* broadband imaging (3CR data taken from de Koff et al. 1996). The three detailed correspondence sources are not included in the CSS sample.

TABLE 2

ALIGNMENT CLASSIFICATION

Category	Total	Quasars	Galaxies
Detailed correspondence[a]	3	3C 380	3C 213.1, 3C 346
Global alignment	13	3C 138, 3C 216, 3C 277.1, 3C 455	3C 49, 3C 67, 3C 237, 3C 266, 3C 268.3, 3C 299, 3C 303.1, 3C 305.1, 3C 343.1
Undetermined	14	3C 43, 3C 147, 3C 186, 3C 190, 3C 191, 3C 286, 3C 287, 3C 298, 3C 309.1, 3C 343, 3C 454	3C 93.1, 3C 119, 3C 258

[a] All sources in the detailed correspondence category are larger than the 20 kpc upper limit to the CSS size.

from ground-based observations (McCarthy et al. 1995), the low-redshift FR II data are also taken with WFPC2 (de Koff et al. 1996), eliminating possible resolution effects.

Figure 3 shows the emission lines as a function of redshift that are present in the broadband F702W filter. Because of the wide bandwidth of the filter, significant amounts of line emission may be present in many of the source images. This uncertainty about whether the emission in the images is due to stellar continuum, line emission, or a combination of both makes it impossible to tell from these images alone what the origin of the aligned component is. A small and incomplete list of the possible mechanisms includes (1) nuclear light, unobscured along the radio axis, scattered into the line of sight (e.g., Fabian 1989; di Serego Alighieri et al. 1989; Dey et al. 1996); (2) gas photoionized by the nucleus in an "ionization cone" aligned with the radio axis (e.g., Neeser, Meisenheimer, & Hippelein 1997); (3) jet-induced star formation (e.g., McCarthy et al. 1987; Rees 1989), in which shocks due to jet–ambient medium interactions trigger star formation, thus delineating the radio structure; or (4) emission-line gas, shock ionized by the radio jets (e.g., Begelman 1998, hereafter BDO97). The fourth mechanism is the only one with a short timescale; in other words, shock-induced line emission indicates ongoing interaction between the radio and the ambient gaseous medium. In the other three scenarios, the radio structure may long since have expanded beyond the optically aligned structure. In this sense, shock-induced line emission is not the preferred alignment mechanism in the large-scale FR II sources, in which the radio structure has expanded well into the intergalactic medium. This is not to say that gas may not continue to interact with the radio structure in these sources, however.

These scenarios make different and testable predictions. A young stellar population should be observable if jet-induced star formation is present. Scattered nuclear light will exhibit a continuum spectral shape, possibly with significant polarization. Finally, strong emission lines will be the signature of shock-powered line emission. We discuss spectroscopic constraints on the nature of the aligned light. First we examine results of KPNO[3] long-slit spectroscopy by Gelderman & Whittle (1994, hereafter GW94), and next we discuss constraints from the Linear Ramp Filter observations.

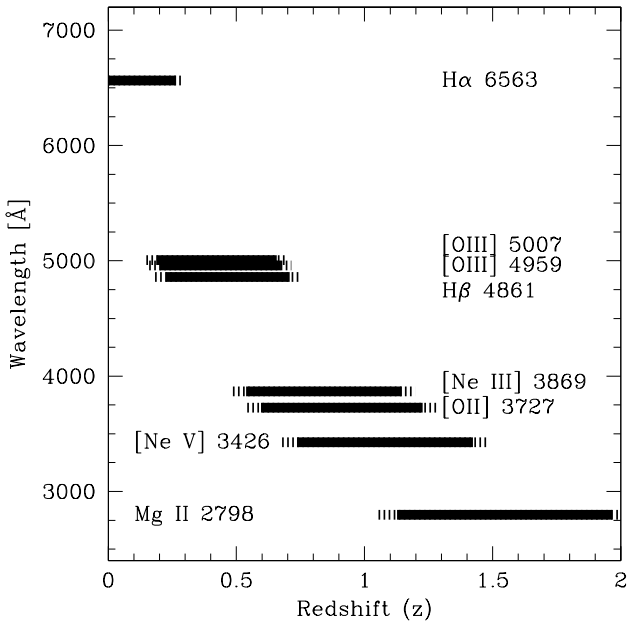

FIG. 3.—Possible emission lines in the WFPC2 F702W passband as a function of redshift. The hatched areas denote the wings of the passband. The relative importance of individual lines may vary strongly between sources.

3.2. *Ground-based Spectral Information*

We estimate the fraction of the light in the F702W filter that is due to emission lines ($f^{\rm line}_{\rm F702W}$), using spectroscopic data where available. Since there is no spatial information in the available ground-based data, we cannot reliably quantify the origin of the aligned component, but a large $f^{\rm line}_{\rm F702W}$ would be consistent with line-emitting gas producing the alignment effect. On the other hand, a particularly low fraction would argue against a line-emission scenario. The emission-line data are taken from GW94, who obtained spectra for 14 CSS sources in our sample. As a first-order approximation, we assume the continuum to be constant across the F702W passband. This way, the equivalent widths of the various lines can be directly added to yield a total equivalent line width within the F702W passband. For almost all the sources considered, this assumption is reasonable (cf. Table 5 in GW94 for continuum fluxes). The calculated equivalent width of the F702W passband, convolved with the system response, is $\sim$1650 Å. Therefore, the line emission fraction, $f^{\rm line}_{\rm F702W}$, in the passband is given by the sum of the equivalent widths of the emission lines, divided by 1650 Å. The data are presented in Table 3, columns (4) to (7). Quoting a 1 σ error on $f^{\rm line}_{\rm F702W}$ is rather difficult, due to the many uncertainties that enter into the calculation. The approximate uncertainties given for the input equivalent widths are on the order of 25% (from GW94), so the resulting uncertainties in the fraction (listed in col. [7]) should be at least as large, and may be significantly larger.

Our assessment of whether emission lines are likely to contribute significantly to the aligned light is given in column (8) of Table 3. The sources with good global alignment between the radio and optical tend to also have significant amounts of line emission (e.g., 3C 67, 3C 93.1, 3C 268.3, 3C 277.1, 3C 303.1, and 3C 455). On the other hand, the sources that do not show evidence for significant line emission tend to be those that are too large to be true CSS sources (see § 2) and/or those that have a detailed optical-radio correspondence (e.g., 3C 213.1, 3C 216, 3C 346, and 3C 380). This strengthens the hypothesis that the alignment effect in the true CSS sources is mostly due to line emission. These results are discussed further in the context of our Linear Ramp Filter observations (§ 5.1).

3.3. *Differences Between CSS Quasars and Galaxies*

The low fraction of quasars with a classifiable alignment (see Table 2), in contrast to the easily categorized galaxies, is illustrative of the problems faced in decomposing the heavily PSF-dominated images into a nuclear and non-nuclear component. Unless we are comparing apples and oranges, the high level of alignment in CSS galaxies should also be present in the CSS quasars. With the exception of 3C 277.1, the F702W quasar images do not show any emission clearly not belonging to the nuclear PSF structure.

[3] Kitt Peak National Observatory, NOAO.

TABLE 3

INFERRED LINE EMISSION IN F702W IMAGES OF CSS SOURCES

3CR Designation (1)	Type[a] (2)	z (3)	EW(O III 5007)[b] (Å) (4)	F702W[c] (%) (5)	Other Lines[d] (6)	Total[e] (%) (7)	LE[f] (8)
3C67	G	0.310	390	23.6	8.2 O III 4959		
					5.5 Hβ 4861	37 ± 9	yes
3C93.1	G	0.243	175	10.6	3.2 O III 4959		
					1.2 Hβ 4861		
					2.5 O I 6300		
					~5 Hα 6563	23 ± 6	yes
3C138	Q	0.759	205	...	...	...	?
3C147	Q	0.545	115	6.9	1.7 Hβ 4861	9 ± 2	?
3C213.1	G	0.194	31	1.3	...	...	no
3C216	Q	0.670	<9	...	...	...	no
3C268.3	G	0.371	130	7.8	1.5 Hβ 4861		
					2.9 O III 4959	12 ± 3	yes
3C277.1	Q	0.321	205	12.4	7.5 Hβ 4861		
					4.0 O III 4959	24 ± 6	yes
3C286	Q	0.849	100	...	0.6 O II 3727		
					0.6 Ne III 3869		
					0.7 other	2 ± 1	?
3C303.1	G	0.267	416	25.2	3.5 Hβ 4861		
					8.8 O III 4959	38 ± 10	yes
3C343.1	G	0.750	71	...	...	...	?
3C346	G	0.161	16	...	...	...	no
3C380	Q	0.692	65	...	0.7 O II 3727		
					0.9 Ne III 3869	2 ± 0.5	no
3C455	Q?	0.543	400	24.2	4.8 Hβ 4861		
					4.8 O III 4959	34 ± 9	yes

[a] Q: quasar; G: galaxy.

[b] Observed equivalent width (±25%); KPNO data are taken from GW94.

[c] Fractional contribution of O III 5007 Å to F702W passband, provided that the line is redshifted into the passband.

[d] Other lines contributing to F702W passband.

[e] Total fractional contribution of lines inside the F702W passband. Errors are estimates.

[f] Alignment possibly due to line-emitting gas.

Using sophisticated PSF modeling software, developed by McLure et al. (1998), on the lowest-z quasar of our sample (3C 147) did show some faint residual structures resembling the ones found in the deep narrowband image of Axon et al. (1999). For the more distant quasars, with their even fainter underlying hosts, identifying real features in the residuals without the help of a deep narrowband image of the same field is impossible. Our efforts to recover any information about nonnuclear quasar emission and to test whether these can be compared to the (aligned) extranuclear emission of the galaxies are described in de Vries (1999, p. 79).

The main results from this comparison are that the underlying host galaxies of CSS galaxies and quasars are of similar brightness and seem to follow the same redshift-luminosity relation. This is consistent with the standard quasar-galaxy viewing angle unification scheme. Any definite statements about whether CSS quasars typically have aligned components will have to be deferred until higher quality imaging data are available.

4. LINEAR RAMP FILTER DATA

Here we present the rest-frame [O III] or [O II] emission-line imaging. The Linear Ramp Filter (LRF), in combination with the WFPC2 instrument, provides a tunable narrowband imaging option well suited for our purposes. A detailed description of LRFs can be found in the WFPC2 instrument handbook (Biretta et al. 1996a).

All observations were carried out as part of the 3CR radio galaxy snapshot program (PI: W. B. Sparks) during cycle 5 (e.g., de Koff et al. 1996; McCarthy et al. 1997). In this specific part of the program (*HST* proposal 05957), the sources were observed between 1995 August and 1996 April with the WFPC2 and one of the LRFs, depending on the redshift of the source. Each source was exposed for 2 × 300 s to make cosmic ray rejection a straightforward process. We list the observed sources and the redshifted emission lines in Table 4.

The LRFs contain four strips per CCD chip, along which the central wavelength varies linearly along the chip with a passband FWHM of ~1.3%. When a source with a specific redshift is to be imaged in rest-frame [O III] line-emission light, the proper LRF and position on either one of the WFPC2 chips is determined. For our subsample, we used the LRFs FR533N, FR680N, and FR868N; in some cases with an additional partial rotation (see also col. [2] of Table 4). As a consequence of the position-wavelength dependence of the setup, all our sources were imaged in one of the Wide Field chips, with their 0.″0996 pixel^{-1} scale.

We followed the LRF reduction procedure given by Biretta, Baggett, & Noll (1996b). There are no flat-field reference files for the LRFs, so we flat-fielded the LRF images with flats created for the narrowband filters closest in wavelength (F588N, F673N, and F791N, respectively). The two exposures for each source were combined using the IRAF/

TABLE 4

LINEAR RAMP FILTER RESULTS

Source (1)	LRF (2)	Line[a] (3)	Factor[b] (4)	Total Flux[c] (5)	Error (%) (6)	Line Flux[d] (7)	Error (%) (8)	Model[e] (9)	Line Flux[f] (10)	L^g_{line} (11)	GB Line Flux[h] (12)	Reference (13)
3C 49	fr680n	O II	0.029	0.47	12	0.34	20	0.262	2.3 ± 0.5	42.3	3.5	2
3C 93.1.....	fr680n	O III	0.043	2.11	2.5	1.09	5.7	0.367	7.2 ± 0.4	42.0	9.0	1
3C 213.1[i].....	fr533n	O III	0.019	0.91	8	0.10	109	0.182	1.3 ± 1.4	41.0	9.0	1
3C 266	fr868n	O II	0.032	0.58	15	0.51	12	0.222	4.2 ± 0.5	43.3		
3C 268.3	fr680n18	O III	0.043	2.13	5.0	1.41	4.7	0.385	8.8 ± 0.4	42.4	5.7, 6.6	1, 3
3C 277.1	fr680n	O III	0.050	9.04	1.0	4.61	1.7	0.403	27.6 ± 0.5	42.8	34.2	1
3C 299[i].....	fr680n18	O III	0.043	5.50	2.0	3.16	2.8	0.392	19.4 ± 0.5	42.8	10.1	3
3C 303.1	fr680n	O III	0.044	4.74	1.3	3.08	2.1	0.402	18.5 ± 0.4	42.5	31.5, 29.5	1, 3
3C 305.1	fr868n33	O II	0.040	0.51	12	0.37	19	0.288	2.3 ± 0.4	42.9	4.8	3
3C 343.1	fr680n	O II	0.051	0.56	10	0.21	32	0.448	0.8 ± 0.3	42.1	1.1	1
3C 380[i].....	fr680n	O II	0.044	5.86	1.1	0.59	12	0.389	2.7 ± 0.3	42.5	2.7, 3.3, 1.9	1, 2, 4

NOTE.—Some loss of signal in the short LRF exposures is to be expected, so on average the LRF values should be (and are) lower than the spectral values. The source 3C 93.1 was imaged in a vignetted area, with up to 10% additional light loss, so the listed value is likely to be an underestimate. The only source with a significant disagreement between the two flux values is 3C 213.1. If the ground-based [O III] flux of 9×10^{-15} ergs s^{-1} cm^{-2} (GW94) were concentrated around the nucleus of the host galaxy, the LRF filter image would have been adequately exposed to show this. In this case, the line-emitting gas is most probably distributed rather evenly over the host galaxy, causing the surface brightness to drop below the detection limit in these shallow (600 s) images.

As a consistency check on our results, we calculate the fractional contribution of line emission to the LRF fluxes in the following way. The line emission fraction (LEF) is: $\mathrm{LEF} = \mathrm{CR_{line}}/\mathrm{CR_{total}}$, where CR is the count rate for the line and total fluxes (cols. [7] and [5] respectively). For the GW94 data, the fractional contribution of emission lines to the LRF fluxes are given by $\mathrm{LEF_{gw94}} = \mathrm{EW_{line}}/(\mathrm{EW_{line}} + \mathrm{EW_{LRF}})$, where EW is the equivalent width. The uncertainty is again taken to be on the order of 25%. The fractional contributions are shown in Fig. 5. Again, the GW94 spectroscopy and the LRF results are in agreement (within the large errors), showing that aligned component is most likely due to line emission.

[a] Rest-frame emission line (either O III 5007 Å or O II 3727 Å) in which the source is imaged.

[b] Conversion factor to normalize the counts pixel^{-1} s^{-1} of the F702W image to the LRF counts pixel^{-1} s^{-1}, after matching the F702W and LRF pixel scales.

[c] LRF continuum + lines flux of source (in counts s^{-1}).

[d] Line flux (in counts s^{-1}), as measured from the lines-only image, constructed from the LRF and the normalized F702W image (applying col. [4]).

[e] SYNPHOT model line flux (counts s^{-1}) for [O III] doublet emission of $2.412.41 \times 10^{-15}$ ergs s^{-1} cm^{-2}, or [O II] emission of 1.81×10^{-15} ergs s^{-1} cm^{-2}, whichever applies to the source.

[f] Line flux (10^{-15} ergs s^{-1} cm^{-2}).

[g] Logarithm of the line luminosity in ergs s^{-1}. Uncertainties are comparable to fractional errors in col. (7).

[h] Ground-based line flux (in units of 10^{-15} ergs s^{-1} cm^{-2}).

[i] Source is larger than the 20 kpc cutoff for CSS sources.

REFERENCES.—(1) Gelderman & Whittle 1994; (2) Jackson & Browne 1991; (3) McCarthy et al. 1995; (4) Lawrence et al. 1996.

STSDAS task CRREJ in order to remove cosmic rays. We calibrated the system throughput using the IRAF SYNPHOT package. Preliminary on-orbit calibration of the LRFs by the STScI WFPC2 group suggests that SYNPHOT provides photometry good to about 8% (C. P. O'Dea, M. McMaster, & J. Biretta, in preparation).

Significant continuum emission can be present in the LRF images, making continuum subtraction necessary. Thus, we removed the continuum emission from the WF/LRF images using scaled PC/F702W images (from Paper I). First, we rebinned the PC data onto the larger WF pixels. Next, we normalized the LRF and F702W images to the same sensitivity. We used the CALCPHOT task in SYNPHOT to calculate the expected count rates (i.e., the normalization factor) given the source spectrum and WFPC2 sensitivity. Ground-based data (GW94) show most of the CSS spectra to be reasonably flat [in (λ, F_λ) plots] over the F702W passband, so we applied the parameters listed in Table 5, redshifted to the appropriate source value. The CALCPHOT factors obtained in this way are listed in column (4) of Table 4, along with other derived quantities.

TABLE 5

CALCPHOT INPUT SPECTRAL PARAMETERS

Parameter	Value
Line fluxes:	
O II 3727.....	7.5×10^{-16} ergs s^{-1} cm^{-2} Å^{-1}
O III 4959.....	2.5×10^{-16} ergs s^{-1} cm^{-2} Å^{-1}
O III 5007.....	7.5×10^{-16} ergs s^{-1} cm^{-2} Å^{-1}
Zero points:	
ZP(O II).....	1.81×10^{-15} ergs s^{-1} cm^{-2}
ZP(O III).....	2.41×10^{-15} ergs s^{-1} cm^{-2}
Line FWHM.....	17 Å
Continuum flux.....	5.0×10^{-16} ergs s^{-1} cm^{-2} Å^{-1}

Constructing line emission and continuum-only images from the F702W and the LRF image is straightforward. In equation form, the line emission–only image is given by $I_{\mathrm{line}} = I_{\mathrm{LRF}} - F_{\mathrm{norm}} I_{\mathrm{F702W}}$, and the continuum-only image by $I_{\mathrm{cont}} = F_{\mathrm{norm}} I_{\mathrm{F702W}} - I_{\mathrm{line}}$. As a consequence, I_{line} and I_{cont} are correlated. Changing the correction factor F_{norm} will give more (or less) line emission and less (or more) of a continuum. This factor can change significantly ($\sim$25%) if, instead of a continuum-plus-line model input spectrum, a pure continuum spectrum is used. Such a model underestimates the flux in the LRF due to the lines, and as a result, the lower F_{norm} yields an I_{line} image with less flux. Since there is clearly line emission left, an iterative modification of the input model spectrum converges to an optimal solution. For some of the fainter sources, however, the images (and the derived fluxes) are not well determined.

5. NARROWBAND IMAGES AND SOURCE DESCRIPTIONS

The images presented in Figures 4*a*–4*k* are constructed as described in § 4. For each source, the left panel shows the

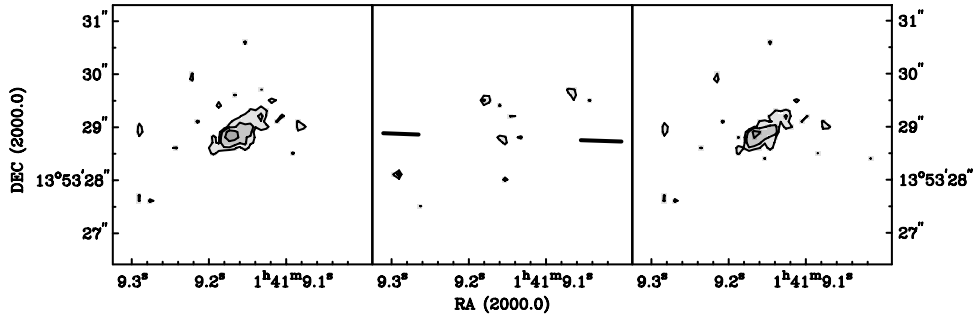

FIG. 4*a*

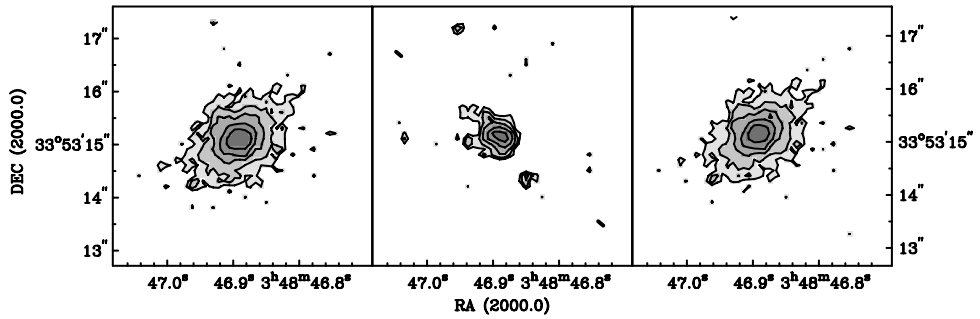

FIG. 4*b*

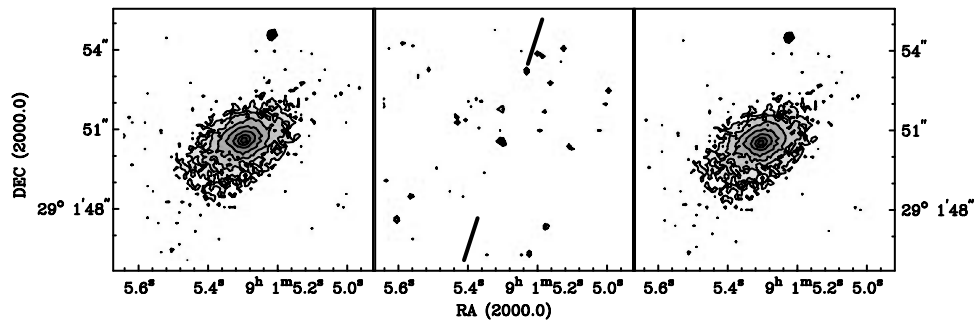

FIG. 4*c*

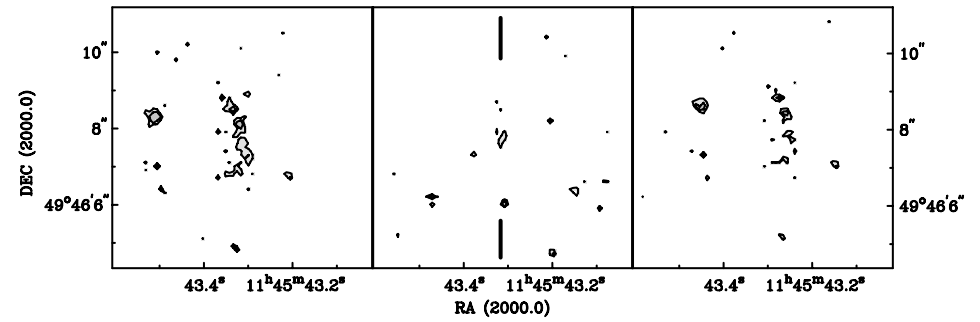

FIG. 4*d*

FIG. 4.—Source images. F702W image is to the left, continuum-only image to the right. [O II] or [O III] line emission is in the middle. The orientation of the radio structure is indicated in the middle panel by the solid bars. The bar length indicates how well the radio orientation is defined. (*a*) 3C 49, imaged in [O II]. (*b*) 3C 93.1, imaged in [O III]. (*c*) 3C 213.1, imaged in [O III]. (*d*) 3C 266, imaged in [O II]. (*e*) 3C 268.3, imaged in [O III]. (*f*) 3C 277.1, imaged in [O III]. (*g*) 3C 299, imaged in [O III]. (*h*) 3C 303.1, imaged in [O III]. (*i*) 3C 305.1, imaged in [O II]. (*j*) 3C 343.1, imaged in [O II]. (*k*) 3C 380, imaged in [O II].

F702W image, rescaled to the lower Wide Field resolution, the middle image shows $I_{\rm line}$, and therefore presumably line emission only, and the right image shows $I_{\rm cont}$, continuum only. Because of the similar exposure times, the F702W image, with its broader passband, has a higher signal-to-noise ratio, and usually more contours, than the middle image. The contour spacing differs between the F702W and the line emission images. However, the F702W and the continuum-only images do have the same spacing. The orientation of the radio structure is indicated in the middle

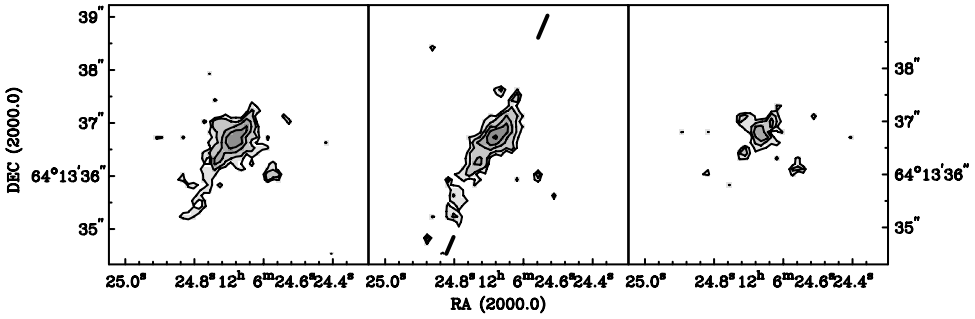

FIG. 4*e*

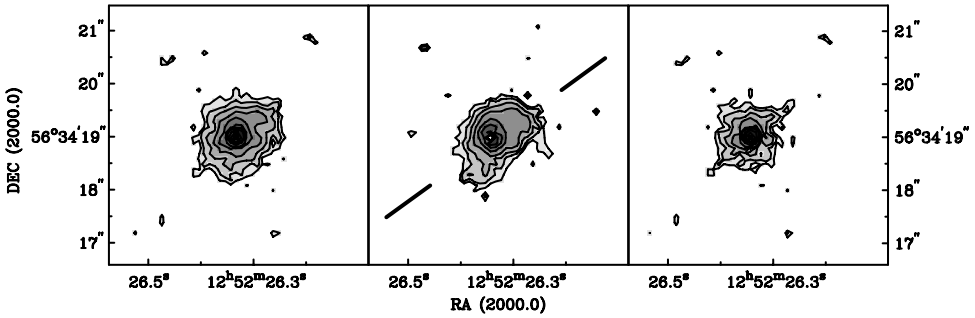

FIG. 4*f*

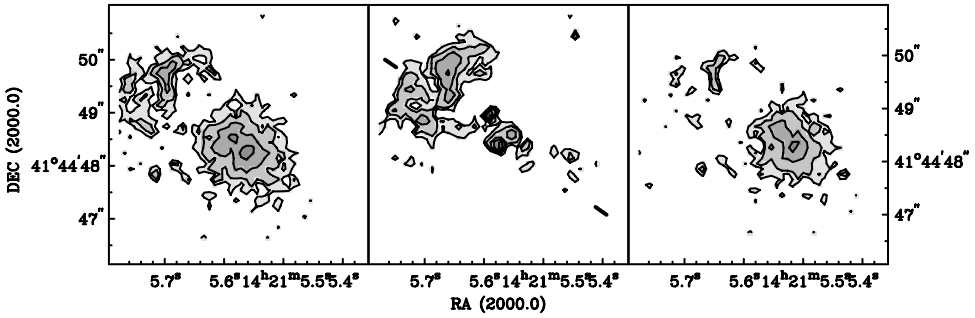

FIG. 4*g*

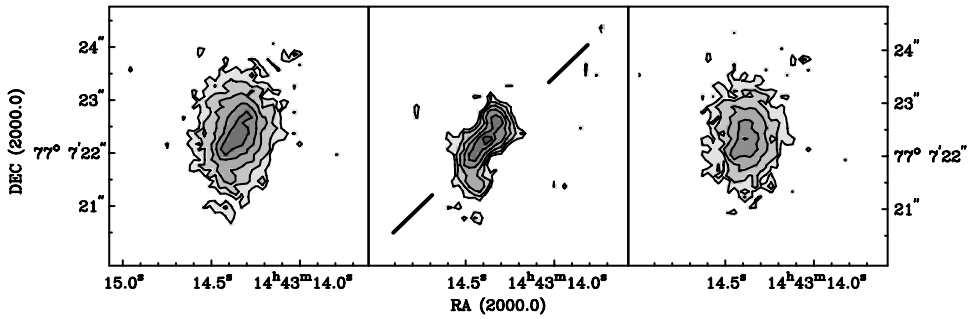

FIG. 4*h*

panel, with the length of the pointer bars as an indication of how well this direction is defined.

3C 49.—[O II], $z = 0.621$. Very faint, diffuse [O II] emission is present in the $I_{\rm line}$ image.

3C 93.1.—[O III], $z = 0.243$. The line emission seems to extend perpendicular to the galaxy's major axis, consistent with the radio image (Paper I).

3C 213.1.—[O III], $z = 0.194$. KPNO spectra indicate the presence of line-emitting gas (GW94), but this is apparently of low surface brightness, so that it does not show up in these shallow images. Both optical hot spots (2.″5 south-southeast and 4″ north-northwest relative to the core; cf. radio-optical image in Paper I) are not detected in $I_{\rm line}$, suggesting that the F702W emission is due to optical continuum.

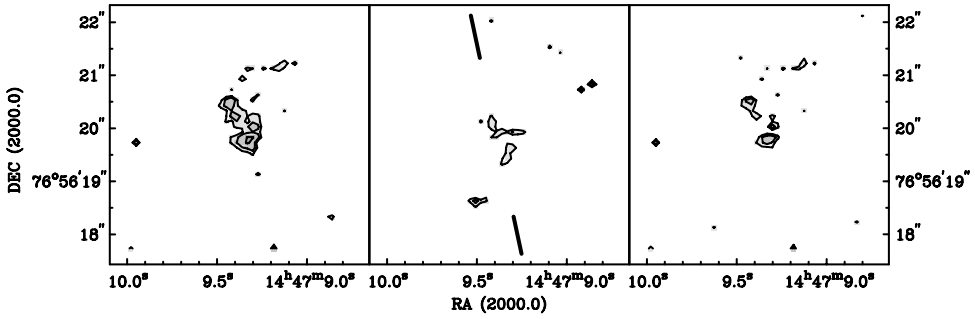

FIG. 4*i*

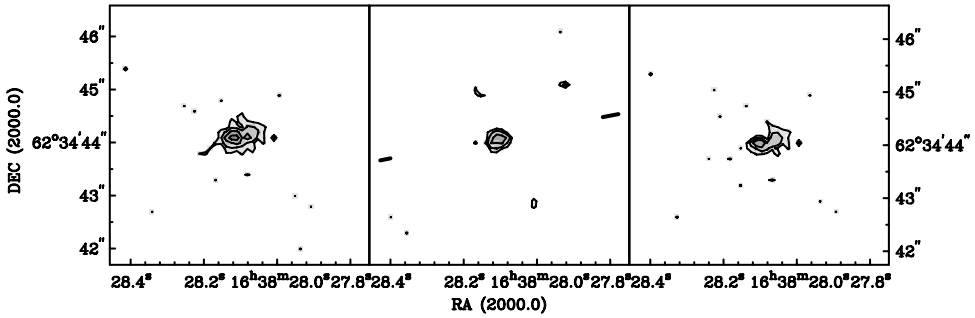

FIG. 4*j*

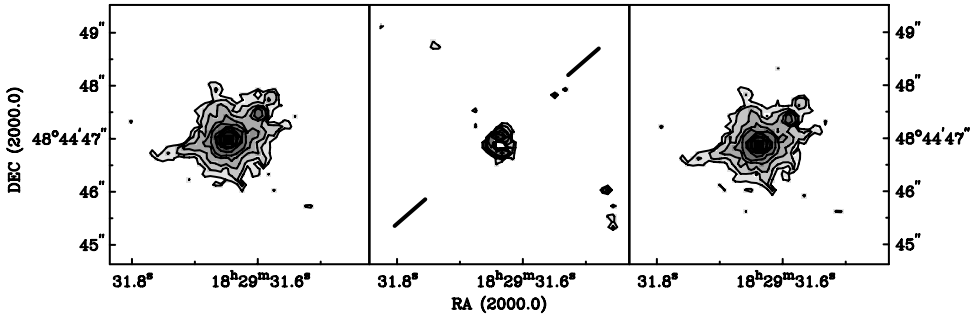

FIG. 4*k*

3C 266.—[O II], $z = 1.275$. This high-redshift galaxy is only marginally detected in [O II]. The faintness of the source, coupled with the decrease in detector sensitivity toward 1 μm, makes deeper exposures a necessity.

3C 268.3.—[O III], $z = 0.371$. A clear aligned component can be seen in the $I_{\rm line}$ image. The decomposition into line and continuum images makes it clear in this case that the aligned component is dominated by line emission, since the continuum emission is confined to the nuclear region.

3C 277.1.—[O III], $z = 0.321$. This is one of the few quasars in our sample with obvious extended emission (Paper I), which is aligned with the radio structure. The continuum image is almost indistinguishable from a pure PSF, implying that the non-PSF emission is due to line emission. These results are consistent with the deeper images in Axon et al. (1999).

3C 299.—[O III], $z = 0.367$. This source has a very asymmetric radio structure, with lobe-nucleus separations of 2.″6 and 13″, respectively (Liu & Pooley 1991; van Breugel et al. 1992). Thus, 3C 299 is not a true CSS source. These images show the closer lobe, in which prominent line emission is detected. The filamentary or shell-like structures to the northeast are due to line emission, whereas most of the underlying host galaxy is continuum emission ($I_{\rm cont}$). Because of problems with precise image alignment, however, some of the filamentary structure is still present in the continuum image.

3C 303.1.—[O III], $z = 0.267$. The line emission is aligned with the radio structure, unlike the underlying host galaxy (Paper I). Thanks to the high signal-to-noise ratio in the LRF and F702W images, we were able to (almost) completely remove the aligned signature from the continuum image. The galaxy seen in $I_{\rm cont}$ is much closer to a regular elliptical than seen in the original F702W image. The deeper images of Axon et al. (1999) show that the faint southern extension is real, indicating that the emission-line gas extends beyond the radio source.

3C 305.1.—[O II], $z = 1.132$. This source is slightly brighter in [O II] than 3C 266, which has a similar redshift. Continuum and line-emission symmetry axes have the same position angle, and are both aligned with the radio structure (Paper I).

3C 343.1.—[O II], $z = 0.750$. The emission is very strongly centrally concentrated (unlike some of the other sources imaged in [O II], notably 3C 266 and 3C 305.1). However,

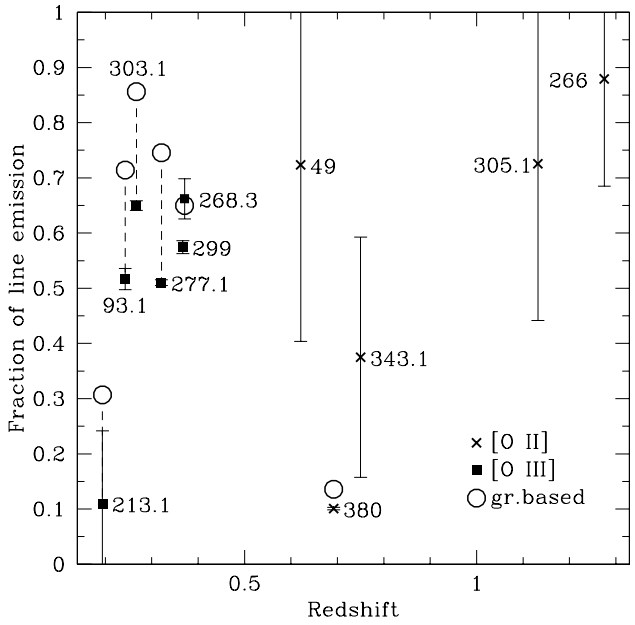

FIG. 5.—Plot of the relative contribution of line emission in the LRF filter, after the continuum has been subtracted. Sources are indicated by their 3CR number. The dashed lines connect the different points for the same source.

the continuum is elongated in the same sense as the radio structure.

3C 380.—[O II], $z = 0.692$. This quasar is classified in the "detailed correspondence" category because of the precise match of the nucleus and both hot spots in the radio and optical images. The lack of line emission suggests that the optical emission is pure continuum. O'Dea et al. (1999a) suggest that the optical hot spots are most likely due to synchrotron radiation from the same population of electrons that produces the strong radio hot spots.

5.1. *Line Fluxes and Luminosities*

We converted the line fluxes in our pure emission line images to customary units with the IRAF task CALCPHOT. Instead of using a continuum-plus-lines model input spectrum, as we did in § 4, we use a model spectrum consisting of just the [O II] 3727 or the [O III] doublet line contribution. The same 17 Å FWHM and the same peak fluxes (Table 5) are assumed. With the measured count rate (CR_{line}), the model count rate (CR_{model}, calculated with CALCPHOT and the input spectra, listed in col. [9] of Table 4), and these zero points, the line flux is given by $F_{line} = CR_{line}/CR_{model}ZP([O\ III]\ or\ [O\ II])$.

Measured fluxes (in counts s^{-1}), with their appropriate errors, are listed in Table 4, columns (5)–(8). The line flux in conventional units is listed in column (10), which can be directly compared to existing ground-based data (col. 12). These values are based on long-slit spectra, typically well exposed and with a slit wide enough to accommodate most of the source (GW94). The line fluxes estimated from the WFPC2/LRF images are generally in good agreement with those estimated from the GW94 spectroscopy (cf. Fig. 5 and the notes to Table 4).

6. THE NATURE OF THE ALIGNED COMPONENT

Our results are summarized in Table 6. Sources with a detailed, one-to-one optical-radio correspondence also have very little line emission in the aligned component, indicating that the alignment is due to continuum emission. In these sources, we suggest that the optical hot spots are due to optical synchrotron emission. Support for this picture has been given for 3C 380 (O'Dea et al. 1999a) and 3C 346 (Dey & van Breugel 1994). In addition, these sources have larger radio structures (>20 kpc) and are not true sub-galactic–scale CSS sources.

TABLE 6

CLASSIFICATION OF ALIGNED LIGHT BASED ON LRF RESULTS

Source	Alignment Classification	Proposed Mechanism	Flux Fraction[a] (%)
3C 49	global	line emission	70
3C 93.1	global	line emission	50
3C 266.....	global	line emission	90
3C 268.3.....	global	line emission	65
3C 277.1.....	global	line emission	50
3C 299.....	global	line emission	60
3C 303.1.....	global	line emission	65
3C 305.1.....	global	line emission	70
3C 343.1.....	global	line emission	40
3C 213.1[b].....	detailed	optical synchrotron	<10
3C 380[b].....	detailed	optical synchrotron	<10

[a] Approximate fraction of line emission in LRF image.
[b] Source is larger than the 20 kpc cutoff for CSS sources.

The "global" alignment CSS sources are consistent with most of the aligned light being line emission. The generally cospatial optical and radio emission suggests that the interaction of the radio source with the ambient gas is responsible for the morphology and possibly the energetics of the emission-line gas.

A natural consequence of the shock-induced line emission scenario is that the radio and line-emission structures should have similar morphologies. In order to quantify source asymmetry, we constructed mean line-emission profiles in Figure 6 both parallel and perpendicular to the source axis for the four sources with bright emission in the LRF and a well-defined core position. The difference between these profiles constrains asymmetric structure and its associated line flux. An almost symmetric source like 3C 93.1 yields a difference curve with no signal in it, while the very elongated structure of 3C 303.1 shows up as two distinct line-emission peaks in the profile. The largest angular extent of the radio structure is indicated in Figure 6 by the filled squares, whose size can be interpreted as the estimated uncertainty in the angular size determination, since some radio images may not represent the total extent of the source (cf. Paper I). These profiles, plus the overlays in Paper I, show that the radio sources seem to straddle the emission-line structure. However, Axon et al. (1999) present deep LRF images of five CSS sources and find that in four of the five, very faint emission line gas extends beyond the observed radio source.

6.1. *The Source of Ionization*

Since these radio sources are sub-galactic in size, they will naturally interact with dense gas as they propagate through the host galaxy. The gas will be compressed and swept up by the radio source and photoionized by the nuclear continuum. There may also be a contribution by in situ ionization from shocks driven by the radio source (BDO97). The relatively high line-emission luminosities and the broad and

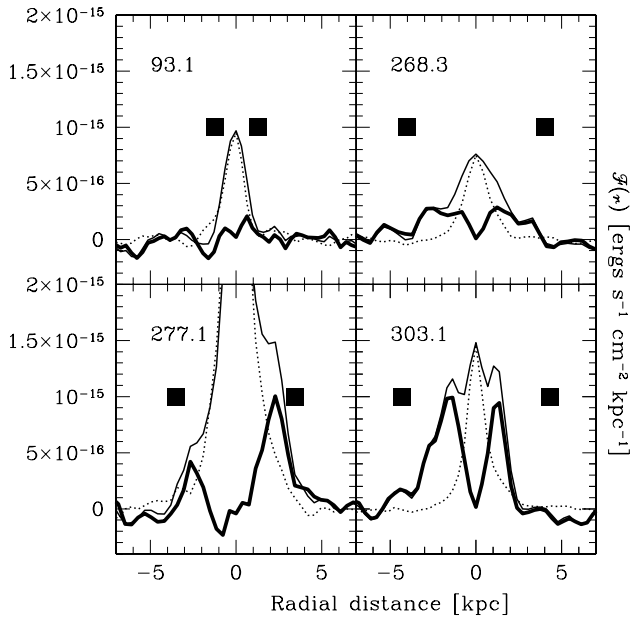

FIG. 6.—Average line emission profiles for four sources of our sample (their 3C number is given in the top left corner). The dashed line represents the profile perpendicular to the radio structure position angle, the solid line is the parallel profile. The thick solid line shows the difference between both lines. The largest extent of the radio source is indicated by the filled squares.

complex [O III] profiles in CSS objects (GW94) argue in favor of strong radio-ISM interactions.

If the sources are ionized by a powerful central source, a strong ionizing continuum must be incident on the clouds close to the radio structure. We might expect that some fraction of the ionizing continuum will scatter off the clouds, producing a polarized UV continuum. A typical value of polarization for some aligned 3C sources with scattered nuclear light is $\sim 10\%$ around 3000 Å (e.g., Cimatti et al. 1997), a value that is rarely attained in GPS and CSS sources (cf. Table 7 of O'Dea 1998). However, the relative geometry in CSS sources may be less favorable for scattering toward us compared to the large-scale sources, being so much more compact. These geometric factors may influence the amount of detectable polarization, even if the amount of scattering is comparable. We furthermore note that analysis of *ROSAT* and *ASCA* observations of the GPS galaxy 2352+495 suggests that there may not be enough nuclear ionizing photons to power the emission-line nebula (O'Dea et al. 1999b). Axon et al. (1999) find that the observed ionizing continuum in two of their CSS galaxies is probably not sufficient to power the observed emission lines. They argue that this is evidence that the ionizing continuum is anisotropic; i.e., the line-emitting nebula sees a stronger continuum than we do. A likely scenario is that the faint emission extending beyond the radio source is photoionized by the active galactic nucleus (AGN), while the brighter line emission within the radio structure has also been energized by shocks.

High-resolution spectroscopy observations with STIS, to determine whether the aligned emission lines are dominated by nuclear or in situ ionization, are in progress.

6.2. *Cooling Length*

Based on Figure 6 and the LRF images, we can conclude that (1) there is a gap between the radio hot spot and the onset of line emission, which implies the absence of a luminous bow shock, and (2) the line emission fills in the area internal to the radio structure and is not confined close to the bow shock. In this section we attempt to explain both points in terms of gas cooling times as a function of local density and shock velocity.

The size differences between the radio and the line-emission structures, as shown in Figure 6, can be interpreted as the time needed for the shocked gas to cool down to the $\sim 10^4$ K temperatures needed for efficient line emission. Substantial work has been done on modeling bow shocks in Seyfert galaxies (e.g., Pedlar, Dyson, & Unger 1985, hereafter PDU85; Wilson & Ulvestad 1987; Taylor, Dyson, & Axon 1992, hereafter TDA92). Applying these models directly to the CSS sources requires some caution, however. The Seyfert galaxies are generally well resolved (a few tens pc resolution) at their low redshifts ($z < 0.05$), compared to the few 100 pc resolution we obtain for the CSS sources. Model details, such as bow shock size and shape, are difficult to constrain at these resolutions. Furthermore, CSS sources are orders of magnitude more radio luminous and exhibit lobe expansion speeds on the order of a few percent of the speed of light (e.g., Readhead et al. 1996b; Owsianik & Conway 1998), a factor of several higher than modeled for Seyfert sources (a few 100 km s^{-1}).

We therefore need to extend the cooling length calculation of TDA92 to include higher shock velocities and lower densities. Following TDA92, we assume that (1) the medium into which the shock will advance is completely ionized, possibly by radiation from the AGN and the bow shock itself, and (2) the size evolution is self-similar, i.e., the lobes can be approximated to first order by an expanding sphere, analogously to the expanding plasmon model of PDU85. The postshock temperature as a function of expansion velocity ($V_{\rm exp}$) is given by

$$T_s = \frac{3}{32}\frac{m_p}{k} V_{\rm exp}^2 , \quad (1)$$

where m_p and k are the proton mass and Boltzmann's constant, respectively. This hot gas will cool both adiabatically and radiatively. We use the TDA92 approximation to the Falle (1975) radiative cooling law, and assume a perfect gas. The overall cooling function (per unit volume) can then be approximated by

$$\frac{dT}{dt} = -aT(t)^b - \frac{3V_{\rm exp}}{R(t)} T(t) , \quad (2)$$

where the first term is the radiative cooling and the second the expansion term. The constants a and b are defined as: for $T > 1.5 \times 10^5$, $a = 0.0333 n_{\rm H}$ and $b = -0.76$; for $T < 1.5 \times 10^5$, $a = 3.98 \times 10^{-13} n_{\rm H}$ and $b = 1.35$, converted from the TDA92 values. Here T_s is taken as the temperature immediately after the shock (at $t = 0$), and $n_{\rm H}$ is the hydrogen number density, assumed to be equal to the electron density for a completely ionized medium. With the expansion, $R(t)$ will increase and therefore reduce the weight of the adiabatic term. In our calculation, the size of the initial shocked region, $R(0)$, has been set to 100 pc.

With shock speeds of ~ 3000 km s^{-1} and densities of 1–5 cm^{-3}, postshock temperatures of a few $\times 10^8$ K are attained, which result in a typical cooling time of $\sim 10^{12}$ s ($\approx 30{,}000$ yr). Assuming a constant expansion speed at least

as large as the shock speed, these timescales result in cooling lengths of a few 100 pc at least. For the four sources presented in Figure 6, three of them (3C 93.1, 3C 268.3, and 3C 277.1) have a $\sim 0.2 \pm 0.2$ kpc gap between the radio and line-emission structures. The source 3C 303.1 has a larger gap of $\sim 1.4 \pm 0.2$ kpc. The lower value of a few 100 pc seems to be consistent with $V_{\rm shock} \gtrsim 1000$ km s^{-1} and $n_{\rm H} \approx$ 1–5 cm^{-3}. The source 3C 303.1 may be an example in which a fast ($\sim 0.02c$) shock is moving into a low-density (< 0.1 cm^{-3}) medium.

In the case of high radio lobe advance speeds (a few 1000 km s^{-1}), the shock front propagates a significant distance in the time it takes the emission-line gas to cool, thus producing an emission-line region that is "cospatial" with a large fraction of the radio source structure. In the case of very slow advance speeds (a few 100 km s^{-1}), the emission-line gas cools before the radio source has propagated very far, and the emission-line gas is concentrated near the leading edge of the radio source. Our LRF images are consistent with the former case, in which the advance speeds are high. This propensity for the sources to have reasonably high $V_{\rm shock}$ and intermediate $n_{\rm H}$ is also consistent with the [O III] emission profiles calculated in TDA92 (cf. their Fig. 3), in which the higher $V_{\rm shock}$ profiles are spatially more extended than the lower $V_{\rm shock}$ profiles for constant density.

The absence of a luminous bow shock, and the inferred $V_{\rm shock}$ of at least 1000 km s^{-1} and density $n_{\rm H} \approx$ 1–5 cm^{-3}, do not agree with the BDO97 model, in which low speeds and high densities are required to maintain a radiative bow shock. The recent expansion velocity determination of $\sim 0.2c$ in a very compact GPS source (Owsianik & Conway 1998) further weakens the BDO97 case for slow shocks in this particular object. However, our results do point toward a shock-ionization origin of the line emission, as proposed by BDO97.

7. SUMMARY AND CONCLUSIONS

Based on our analysis of the *HST*/WFPC2 F702W and LRF data and complementary Kitt Peak spectroscopy (GW94), we conclude the following.

1. CSS sources display high surface brightness light (in F702W) that is aligned with the radio source.

2. The alignment can be classified in two ways: either there is a detailed one-to-one correspondence between optical and radio structures, or there is a more global alignment of both axes. Ground-based spectral information showed these detailed correspondence sources to have far less line emission than the global-alignment sources. This low fraction of line emission, combined with the one-to-one correspondence between the radio and optical structures, is consistent with the hypothesis that their aligned emission is due to optical synchrotron radiation. The high fraction of line emission in the F702W filter in the sources displaying global alignment suggests that this aligned component is due to emission-line gas.

3. Difficulties with proper PSF subtraction and a lack of dynamic range in the current detectors limit assessment of alignment in CSS quasars to a few exceptional cases. Our analysis of PSF-subtracted images as well as a comparison of the flux within and external to a 1 kpc aperture is consistent with the presence of extended light similar to that seen in the radio galaxies. However, we are not able to reliably determine its morphology or orientation. This result is also consistent with the viewing-angle–dependent galaxy-quasar unification scheme.

4. The LRF images presented here show that for the global alignment sources, there is a strong correlation between radio and line-emission structures. The radio structure seems to straddle the bright emission line gas, implying that most of this emission seems to be radiated in the "wake" of the radio plasma. In four cases, there are faint emission lines beyond the radio source. A likely scenario is that the faint emission extending beyond the radio source is photoionized by the AGN, while the brighter line emission within the radio structure has been energized by shocks.

5. Calculation of cooling times based on the observed gap between the radio hot spots and the onset of aligned emission yields a typical CSS lobe expansion speed of $\gtrsim$1000 km s^{-1} (3C 303.1 is most consistent with $V_{\rm shock} \approx$ 6000 km s^{-1}), and an ambient density of 1–5 cm^{-3} (at the size of the radio structure). The expansion speed is higher than predicted by the BDO97 model, but consistent with multiepoch radio observations.

In summary, we find that CSS galaxies show (red) optical light aligned with the radio source (Paper I). Ground-based spectroscopy and LRF observations of either [O III] 5007 Å or [O II] 3727 Å of a subset of these sources suggests this light is predominantly due to emission lines. Axon et al. (1999) have reached similar conclusions. Our observations are consistent with a picture in which the CSS galaxies interact strongly with the ISM of the host galaxy as they propagate through it. Further observations are needed to determine the kinematics and ionization of the aligned emission-line gas in the radio galaxies, and to search for such gas in the quasars.

This work was based on observations made with the NASA/ESA Hubble Space Telescope, obtained from the data archive at the Space Telescope Science Institute. STScI is operated by the Association of Universities for Research in Astronomy, Inc. under NASA contract NAS 5-26555. W. H. D. V. was supported by a grant to C. P. O. from the Director's Discretionary Research Fund. This research made use of (1) the NASA/IPAC Extragalactic Database (NED) which is operated by the Jet Propulsion Laboratory, California Institute of Technology, under contract to the National Aeronautics and Space Administration; and (2) NASA's Astrophysics Data System Abstract Service. We also would like to thank Ross McLure for running his PSF modeling software on 3C 147.

REFERENCES

Axon, D. J., Capetti, A., Fanti, R., Morganti, R., Robinson, A., & Spencer, R. 1999, MNRAS, submitted
Barthel, P. D., Pearson, T. J., & Readhead, A. C. S. 1988, ApJ, 329, L51
Begelman, M. C. 1996, in Cygnus A: Study of a Radio Galaxy, ed. C. Carilli & D. Harris (Cambridge: Cambridge Univ. Press)
———. 1998, in The Most Distant Radio Galaxies, ed. H. J. A. Röttgering, P. Best, & M. D. Lehnert (Dordrecht: Kluwer), in press (preprint astro-ph/9712107)
Bicknell, G., Dopita, M. A., & O'Dea, C. P. 1997, ApJ, 485, 112 (BDO97)
Biretta, J. A., et al. 1996a, WFPC2 Instrument Handbook, version 4.0 (Baltimore: STScI)
Biretta, J. A., Baggett, S., & Noll, K. 1996b, Photometric Calibration of WFPC2 Linear Ramp Filter Data in SYNPHOT (WFPC2 Instrument Science Report 96-06; Baltimore: STScI)
Bogers, W. J., Hes, R., Barthel, P. D., & Zensus, J. A. 1994, A&AS, 105, 91
Carvalho, J. C. 1985, MNRAS, 215, 463

Chambers, K. C., Miley, G. K., & van Breugel, W. J. M. 1987, Nature, 329, 604
Cimatti, A., Dey, A., van Breugel, W., Hurt, T., & Antonucci, R. 1997, ApJ, 476, 677
Cotton, W. D., Feretti, L., Giovannini, G., Venturi, T., Lara, L., Marcaide, J., & Wehrle, A. E. 1995, ApJ, 452, 605
de Koff, S., Baum, S. A., Sparks, W. B., Biretta, J., Golombek, D., Macchetto, F., McCarthy, P., & Miley, G. K. 1996, ApJS, 107, 621
de Vries, W. H. 1999, Ph.D. thesis, Univ. of Groningen (The Netherlands)
de Vries, W. H., O'Dea, C. P., Baum, S. A., Perlman, E., Lehnert, M. D., & Barthel, P. D. 1998a, ApJ, 503, 156
de Vries, W. H., O'Dea, C. P., Perlman, E., Baum, S. A., Lehnert, M. D., Stocke, J., Rector, T., & Elston, R. 1998b, ApJ, 503, 138
de Vries, W. H., et al. 1997, ApJS, 110, 191 (Paper I)
Dey, A., Cimatti, A., van Breugel, W., Antonucci, R., & Spinrad, H. 1996, ApJ, 465, 157
Dey, A., & van Breugel, W. J. M. 1994, AJ, 107, 1977
De Young, D. S. 1993, ApJ, 402, 95
———. 1997, ApJ, 490, L55
di Serego Alighieri, S., Fosbury, R. A. E., Quinn, P. J., & Tadhunter, C. N. 1989, Nature, 341, 307
Eracleous, M., & Halpern, J. P. 1994, ApJS, 90, 1
Fabian, A. C. 1989, MNRAS, 238, 41p
Falle, S. A. E. G. 1975, A&A, 43, 323
Fanti, C., Fanti, R., Dallacasa, D., Schilizzi, R. T., Spencer, R. E., & Stanghellini, C. 1995, A&A, 302, 317
Fanti, R., Fanti, C., Schilizzi, R. T., Spencer, R. E., Nan Rendong, Parma, P., van Breugel, W. J. M., & Venturi, T. 1990, A&A, 231, 333
Gelderman, R., & Whittle, M. 1994, ApJS, 91, 491 (GW94)
Jackson, N., & Browne, I. W. A. 1991, MNRAS, 250, 414
Lawrence, C. R., Zucker, J. R., Readhead, A. C. S., Unwin, S. C., Pearson, T. J., & Xu, W. 1996, ApJS, 107, 541
Liu, R., & Pooley, G. 1991, MNRAS, 253, 669
McCarthy, P. J., Miley, G. K., De Koff, S., Baum, S. A., Sparks, W. B., Golombek, D., Biretta, J., & Macchetto, F. 1997, ApJS, 112, 415
McCarthy, P. J., Spinrad, H., & van Breugel, W. J. M. 1995, ApJS, 99, 27
McCarthy, P. J., & van Breugel, W. J. M. 1989, in The Epoch of Galaxy Formation, ed. C. S. Frenk et al. (NATO ASI Ser. 264; Dordrecht: Kluwer), 57
McCarthy, P. J., van Breugel, W. J. M., Spinrad, H., & Djorgovski, S. 1987, ApJ, 321, L29
McLure, R. J., Dunlop, J. S., Kukula, M. J., Baum, S. A., O'Dea, C. P., & Hughes, D. H. 1998, MNRAS, submitted
Mutel, R. L., Su, B., & Song, S. 1990, in Proc. of the Dwingeloo Workshop on Compact Steep Spectrum and GHz-Peaked Spectrum Radio Sources, ed. C. Fanti et al. (Bologna: Inst. di Radioastronomia), 17
Neeser, M. J., Meisenheimer, K., & Hippelein, H. 1997, ApJ, 491, 522
O'Dea, C. P. 1998, PASP, 110, 493
O'Dea, C. P., de Vries, W. H., Biretta, J. A., & Baum, S. A. 1999a, AJ, 117, 1143
O'Dea, C. P., de Vries, W. H., Worrall, D., & Baum, S. A. 1999b, ApJ, submitted
O'Dea, C. P., & Baum, S. A. 1997, AJ, 113, 148
O'Dea, C. P., Baum, S. A., & Stanghellini, C. 1991, ApJ, 380, 66
Owsianik, I., & Conway, J. E. 1998, A&A, 337, 69
Pedlar, A., Dyson, J. E., & Unger, S. W. 1985, MNRAS, 214, 463 (PDU85)
Readhead, A. C. S., Taylor, G. B., Pearson, T. J., & Wilkinson, P. N. 1996a, ApJ, 460, 634
Readhead, A. C. S., Taylor, G. B., Xu, W., Pearson, T. J., Wilkinson, P. N., & Polatidis, A. G. 1996b, ApJ, 460, 612
Rees, M. J. 1989, MNRAS, 239, 1p
Taylor, D., Dyson, J. E., & Axon, D. J. 1992, MNRAS, 255, 351 (TDA92)
Taylor, G. B., Ge, J., & O'Dea, C. P. 1995, AJ, 110, 522
van Breugel, W. J. M., Fanti, C., Fanti, R., Stanghellini, C., Schilizzi, R. T., & Spencer, R. E. 1992, A&A, 256, 56
Wilkinson, P. N. 1990, in Proc. of the Dwingeloo Workshop on Compact Steep Spectrum and GHz-Peaked Spectrum Radio Sources, ed. C. Fanti et al. (Bologna: Inst. di Radioastronomia), 115
Wilson, A. S., & Ulvestad, J. S. 1987, ApJ, 319, 105